

# Gyrokinetic and kinetic particle-in-cell simulations of guide-field reconnection. Part I: macroscopic effects of the electron flows

P. A. Muñoz,<sup>1, a)</sup> D. Told,<sup>2,3</sup> P. Kilian,<sup>1</sup> J. Büchner,<sup>1</sup> and F. Jenko<sup>2,3</sup>

<sup>1)</sup>Max-Planck-Institut für Sonnensystemforschung, D-37077 Göttingen, Germany

<sup>2)</sup>Max-Planck-Institut für Plasmaphysik, D-85748 Garching, Germany

<sup>3)</sup>Department of Physics and Astronomy, University of California, Los Angeles, CA 90095, USA

(Dated: December 3, 2024)

In this work, we extend a comparison between gyrokinetic (GK) and fully kinetic Particle-in-Cell (PIC) simulations of magnetic reconnection in the limit of strong guide field started by TenBarge *et al.* [Phys. Plasmas **21**, 020708 (2014)]. By using a different set of kinetic PIC and GK simulation codes (ACRONYM and GENE, respectively), we analyze the limits of applicability of the GK approach when comparing to the force free kinetic simulations in the low guide field ( $b_g$ ) regime. Here we report the first part of a much more extended comparison, focusing on the macroscopic effects of the electron flows. For a low beta plasma ( $\beta_i = 0.01$ ), it is shown that magnetic reconnection only displays similar features between both plasma models for higher kinetic PIC guide fields ( $b_g \gtrsim 30$ ) in the secondary magnetic islands than in the region close to the X points or separatrices ( $b_g \gtrsim 5$ ). Kinetic PIC low guide field runs ( $5 \lesssim b_g \lesssim 30$ ) reveal secondary magnetic islands with a core magnetic field and less energetic flows inside of them in comparison to the GK or kinetic PIC high guide field simulations. We find that these processes are mostly due to an initial shear flow absent in the GK initialization and negligible in the kinetic PIC high guide field regime, in addition to fast outflows on the order of the ion thermal speed that violate the GK ordering. Since secondary magnetic islands appear after the reconnection peak time, a kinetic PIC/GK comparison is more accurate in the (early) linear phase of magnetic reconnection. For a high beta plasma ( $\beta_i = 1.0$ ), similar processes happen, but they require lower guide fields ( $b_g \gtrsim 3$ ) to be negligible due to the reduced reconnection rate and fluctuation level.

## I. INTRODUCTION

Magnetic reconnection is a fundamental process in plasma physics that converts magnetic field energy efficiently into plasma heating, bulk flows and accelerated particles. It plays a role in a wide range of different environments, from fusion devices, planetary magnetospheres, stellar coronae to extragalactic accretion disks<sup>1</sup>.

Usually, magnetic reconnection is modeled with antiparallel magnetic fields in a plane sustained by a current sheet (CS). But that configuration is unrealistic, since in nature the presence of a strong out-of-plane magnetic field is ubiquitous in both space and laboratory plasmas, such as in the solar corona and fusion devices, respectively. However, the properties of reconnection in the presence of a guide field are much less understood (see Ref. 2 for a recent review). Thus, the study of stability of these CS with shear magnetic fields is of paramount importance to understand the conversion of magnetic energy in these environments.

In order to capture the kinetic effects in magnetic reconnection, fully kinetic particle-in-cell (PIC) codes have become one of the preferred tools since some time ago, with the increasing availability of computational resources<sup>3</sup>. These codes allow the simulation of magnetic reconnection in fully collisionless Vlasov plasmas. However, these fully kinetic PIC simulations (for brevity, from

now on these ones will be simply referred to as “PIC simulations”) can be computationally very demanding due to stability reasons and the requirement of keeping numerical noise as low as possible. One approach to solve this problem is using gyrokinetic (GK) theory, an approximation to a Vlasov plasma (See Ref. 4 or Ref. 5 for a recent review). In this plasma model, the idea is to decouple the fast gyrophase dependence from the dynamics, considering the motion of charged rings, thus reducing the phase space from six to five dimensions and removing dynamics on very small space-time scales. The gyrokinetic approach is suitable in strongly magnetized plasmas (equivalent to the limit of very large magnetic guide fields in magnetic reconnection). More precisely, the ion gyroradius  $\rho_i$  has to be much smaller than the typical length scale  $L_0$  of the system:  $\epsilon = \rho_i/L_0 \ll 1$ , where  $\epsilon$  is the GK ordering parameter. This also implies the restriction of the GK approach to low frequency phenomena:  $\omega/\Omega_{ci} \sim \mathcal{O}(\epsilon)$ , where  $\omega$  is a typical frequency in the system. The fluctuations in the distribution function and electromagnetic fields, with respect to their equilibrium values, are also of order  $\mathcal{O}(\epsilon)$ . And finally, these fluctuations are assumed to have much larger scales along the magnetic field direction than across it:  $k_{\parallel}/k_{\perp} \sim \mathcal{O}(\epsilon)$ , where  $k_{\parallel}$  and  $k_{\perp}$  are the wavevectors along and across the magnetic field, respectively. An important consequence of this assumption is that the perpendicular bulk speed  $\vec{V}_{\perp}$  is mostly dominated by drifts, which have to be smaller than the ion thermal speed  $v_{th,i}$  according to  $\epsilon = V_{\perp}/v_{th,i} \ll 1$ . This fact will be a source of differences between the GK and kinetic simulations that do not have

<sup>a)</sup>Electronic mail: munozp@mps.mpg.de

such a restriction.

Simulations of magnetic reconnection with codes based in the GK theory have shown to drastically reduce the computation time, which allows the use of more realistic numerical parameters (e.g.: mass ratio), and at the same time, the possibility to capture many of the desired kinetic effects, such as finite ion Larmor radius ones<sup>6-9</sup>. However, one of the drawbacks of the GK simulations of magnetic reconnection is that the initial setup has to be force free  $\vec{J} \times \vec{B} = 0$ . The often used Harris sheet<sup>10</sup> initialization is not possible in the standard gyrokinetic theory, since the particles that carry the current are different from the background, and therefore the perturbed current is of second order in the ordering GK parameter  $\epsilon$ . Nevertheless, a force free initialization is a good approximation to the exact kinetic equilibrium in low beta plasmas with strong guide field.

Due to the previous reasons, it is of fundamental importance to establish the key properties of magnetic reconnection that can be properly modeled with a gyrokinetic code, instead of running computationally expensive fully kinetic PIC simulations. In this context, the first direct comparison between PIC and GK simulations of magnetic reconnection in the large guide field limit was performed just recently by Ref. 11. They found that many reconnection related quantities (such as the reconnection rates) obtained for different PIC guide field runs have the same value after they are scaled to  $b_g$ . And this value is equal to the provided by the GK simulations after a proper choice of the  $\epsilon$  parameter. This is valid under the assumption of a constant total plasma  $\beta$  (to be defined in the next Sec. II) among different PIC guide field runs. The result is in agreement with predictions of the two fluid analysis by Ref. 12. In addition, the morphology of the out-of-plane current density show a good convergence between the PIC simulations with sufficiently high guide field and the gyrokinetic runs. They also noticed that low  $\beta$  plasmas require higher PIC guide fields to reach convergence towards the GK results, in comparison to high  $\beta$  plasmas.

The promising results of the previous benchmark study by Ref. 11 encouraged us to follow their approach and extend their results. Our work complement theirs by investigating the origin of the differences between PIC and gyrokinetic results in the realistic regime of low guide fields (since PIC cannot use arbitrarily large values of guide field, where results should match). In this sense, our main goal is to establish the limits of applicability of the GK simulations in comparison with the corresponding PIC simulations of magnetic reconnection. In addition to numerical differences between the codes related with the pressure equilibrium condition, we will show that the agreement between both breaks down mostly when secondary magnetic islands appear in the PIC simulations. Although they also appear in the PIC high guide field regime or the GK simulations, these secondary magnetic islands have different features as a result of an initial shear flow present in the PIC force free initialization.

The secondary magnetic islands are structures that appear as a result of the tearing mode, with a different (smaller) wavelength than the one imposed by the large scale initial perturbation. They start at electron length scales, growing up to ion scales. In this sense, our definition does not exactly match with some previous studies<sup>13-15</sup>, which limit secondary islands to those ones with electron length scales. Other works have stated that secondary islands have opposite out-of-plane current density to those of the primary islands<sup>16</sup>. Again, the structures in our simulations do not match these features.

We expect the formation of these structures in our setup, since it is known that guide field reconnection produce a “burstier” reconnection, forming more secondary magnetic islands than an antiparallel configuration<sup>17</sup>. Many previous works have analyzed these structures with several level of details, in particular in the context of extended current layers, since they can modulate temporally the reconnection rates (see Ref. 18 and references therein). For example, the authors of Ref. 19 reported a core magnetic field inside of secondary magnetic islands by means of 2D PIC simulations of Harris sheets with weak magnetic guide field. It was attributed to a nonlinear amplification mechanism between the guide field and the Hall term. Later, Ref. 20 analyzed the same phenomenon in a similar setup but with 2D PIC simulations during the coalescence of secondary magnetic islands. In our case, we will show that a similar consequence takes place but as a result of a shear flow initialization in the PIC low guide field regime.

Shear flows have been analyzed exhaustively for their importance in the development of magnetic reconnection. It is known that reconnection rates decrease with faster shear flows parallel to the reconnected magnetic field, according to the scaling law derived in Ref. 21 under a Hall-MHD model without guide field (basically, due to less efficient outflows from the X point). A kinetic approach and PIC simulations have confirmed this prediction, but have also shown that tearing mode (associated with the formation of magnetic islands) is never completely stabilized for thin CS, even with super-Alfvénic flows<sup>22</sup>. A two-fluid analytical study<sup>23</sup> of collisionless tearing mode driven by electron inertia showed that a shear flow, under certain conditions, can generate a symmetric out-of-plane magnetic field. Shear flows are also closely related with the Kelvin-Helmholtz instability. Our PIC runs in the low guide field regime do not exhibit outflows with sufficient speed to drive the kinetic version of Kelvin-Helmholtz, mostly because they scale as the Alfvén speed  $V_A$  which is known to be a threshold for this instability<sup>24</sup>. It is also important to mention the work by Ref. 25, which found secondary magnetic islands generated by the Kelvin-Helmholtz instability in the reconnection outflow. On the other hand, the structures observed in our case appear only close to the main X point. However, the secondary magnetic islands in our PIC/GK simulations share some of the features seen in those previous works.

That is why we are going to relate their appearance with the core magnetic field and shear flow, depending on the parameter regimes of our PIC/GK runs.

The remainder of this paper is organized as follows. In Sec. II, we describe the simulation setup used by both GK and PIC codes, as well as the parameter range to be studied. In Sec. III, we show our reproduction of the results obtained by the first comparison work by Ref. 11. This is done in the context of a linear scaling of magnetic and thermal pressures on dependence on the guide field. The purpose of this section is also to identify where and when the differences between PIC and GK simulation results appear. These differences are manifested in both magnetic and thermal pressure fluctuations. In this paper we focus on the first ones, while the deviations with respect to the linear scaling in the thermal pressure fluctuations will be deferred to a follow-up paper. The remarkably high values of magnetic fluctuations in the PIC low guide field regime are due to the generation of a core magnetic field in the secondary magnetic islands. This process is discussed in Sec. IV in the context of two fluid theory and violations of the pressure equilibrium condition. Then, in Sec. V, we analyze the physical mechanism of this core magnetic field as a result of a shear flow due to the force free initialization in the PIC low guide field runs. We briefly discuss the effects of a high  $\beta$  plasma on all these processes in Sec. VI. Finally, we summarize our findings in the conclusion, Sec. VII.

## II. SIMULATION SETUP

The results of the 2.5D simulations (no variations allowed in the out-of-plane direction  $\hat{z}$ ) to be shown were obtained with the explicit fully kinetic PIC code ACRONYM<sup>26</sup> and the gyrokinetic GENE code<sup>27</sup>. For both PIC and gyrokinetic simulations, we used a very similar setup and parameter set to these used in Ref. 11. We will repeat here the more important parameters to ensure a future accurate reproducibility of our work. The initial equilibrium is a force free double CS, with halfwidth  $L$  and magnetic field  $\vec{B}(x) = B_y(x)\hat{y} + B_z(x)\hat{z}$  given by:

$$\begin{aligned} B_y &= B_{\infty y} \left[ \tanh\left(\frac{x - L_x/4}{L}\right) - \tanh\left(\frac{x - 3L_x/4}{L}\right) - 1 \right], \\ B_z &= B_{\infty y} \left[ b_g^2 + \cosh^{-2}\left(\frac{x - L_x/4}{L}\right) \right. \\ &\quad \left. + \cosh^{-2}\left(\frac{x - 3L_x/4}{L}\right) \right], \end{aligned} \quad (2)$$

with relative guide field strength  $b_g = B_g/B_{\infty y}$ , where  $B_{\infty y}$  is the (asymptotic) reconnected magnetic field. This corresponds to a total magnetic field of constant magnitude  $B_T = B_{\infty y}\sqrt{1 + b_g^2}$ .  $L_x$  and  $L_y$  are the simulation box sizes in the reconnection plane  $x$ - $y$ , respectively. Ions are initially stationary, while the current

| Case      | $\beta_i$ | $\omega_{pe}/\Omega_{ce}$ | $v_{th,e}/c$ | $L/\rho_i$ | $L_x (= L_y)$ |
|-----------|-----------|---------------------------|--------------|------------|---------------|
| Low beta  | 0.01      | 0.8                       | 0.125        | 2          | $40\pi\rho_i$ |
| High beta | 1.0       | 4.0                       | 0.25         | 1          | $20\pi\rho_i$ |

Table I. Physical parameters for the two sets of runs.

is carried by drifting electrons with velocity  $\vec{U}_e$  according to  $\vec{J} = -en_e\vec{U}_e$ , satisfying the Ampère equation  $\nabla \times \vec{B} = \mu_0\vec{J}$ .  $n_e = n_i = n_0$  are the initial constant electron (“e”) and proton (“i”) number densities, respectively. In order to accelerate the reconnection onset, we use a perturbation in  $B_x$  and  $B_y$  that generates an X/O point at the center of the left/right CS and that can be derived from the vector potential  $\delta A_z$

$$\delta A_z = \delta P \frac{L_y}{2\pi} \sin\left(\frac{2\pi(y + L_y/4)}{L_y}\right) \sin^2\left(\frac{2\pi x}{L_x}\right), \quad (3)$$

where  $\delta P = 0.01$  is the amplitude of the perturbation. The parameters used in this study are divided in two sets: “low” and “high” beta cases, being summarized in Table I. All the corresponding quantities are calculated with respect to  $B_T$ , i.e.: the ion plasma beta  $\beta_i = 2\mu_0 n_0 k_B T_i / B_T^2$ , the electron/ion cyclotron frequency  $\Omega_{C\{e/i\}} = eB_T/m_{\{e/i\}}$  and the ion Larmor radius  $\rho_i = v_{th,i}/\Omega_{Ci}$ , with the ion thermal speed  $v_{th,i} = \sqrt{2k_B T_i/m_i}$ . We also have equal temperatures  $T_i = T_e$ . We also have equal temperatures for both species  $T_i = T_e$ . Because of the latter, the three first parameters given in Table I are not independent, but they are related by  $\sqrt{\beta_i} = (\omega_{pe}/\Omega_{Ce})(v_{th,e}/c)$ . This relation justifies the necessary change of the latter parameters between the low and high beta cases. The lengths will be normalized to  $\rho_i$  and the times to the Alfvén time  $\tau_A = L/V_A$ , where  $V_A$  is the Alfvén speed defined with respect to the reconnected magnetic field:

$$\frac{V_A}{c} = \frac{B_{\infty y}}{\sqrt{u_0 n_0 m_i}} = \frac{1}{\sqrt{1 + b_g^2}(\omega_{Pe}/\Omega_{ce})\sqrt{m_i/m_e}}, \quad (4)$$

where  $\omega_{Pe} = \sqrt{n_e e^2/(\epsilon_0 m_e)}$  is the electron plasma frequency. We use the previous definitions for the normalization of the reconnection rate:  $\dot{\psi}_N = B_{\infty y} V_A$  and current density:  $J_N = en_0 V_A / \sqrt{\beta_i} = en_0 v_{th,i} / \sqrt{1 + b_g^2}$ . Note that due to the Ampère’s law, the normalized initial out-of-plane current density that supports the asymptotic magnetic field  $B_y$  will be given by:

$$J_{zN} := \frac{J_z(t=0)}{J_N} = \frac{en_0 U_e}{J_N} = \frac{U_e}{v_{th,i}} \sqrt{1 + b_g^2} = \frac{1}{(L/d_i)\sqrt{\beta_i}}, \quad (5)$$

which is independent on the guide field strength. Many of the PIC quantities will be rescaled (see Sec. III for the physical justification) by the factor

$$\Gamma = \frac{\sqrt{1 + b_g^2}}{b_{g,ref}}, \quad (6)$$

where  $b_{g,ref}$  is a reference guide field, chosen to be  $b_g = 10/5$  in the low/high beta case, respectively. This is done to match with the ordering parameter  $\epsilon$  of the GK runs, defined by:

$$\epsilon = \frac{1}{b_{\infty y, norm} b_{g, ref}}, \quad (7)$$

where  $b_{\infty y, norm} = B_{\infty y} / B_{\infty y, ref}$  is the normalized asymptotic magnetic field with respect to a reference value  $B_{\infty y, ref}$  expressed in code units. The initialization in the GK runs gives  $b_{\infty y, norm} = 0.05/2.5$  for the low/high beta cases, respectively. Therefore, using the aforementioned PIC  $b_{g, ref}$ , we have  $\epsilon = 2/0.04$  for the low/high beta case, respectively.

Both codes use double periodic boundary conditions ( $x$  and  $y$  directions). For the PIC runs, we use a grid size  $\Delta x$  of  $N_x = N_y = 1024$  cells in the low beta case (with  $\rho_e / \Delta x = 1.69$ ), while for the high beta case is  $N_x = N_y = 1280$  cells (with  $\rho_e / \Delta x = 4.07$ ). The time step is chosen to be  $\Delta t \omega_{pe} = 0.03/0.12$  in the low/high beta case, respectively, to fulfill the CFL condition with  $(c\Delta t) / \Delta x = 0.5 < 1$ . 1000 particles per cell are used in both cases for each species. Finally, a TSC shape function and no current smoothing were used. For the GK runs, the spatial grid is  $N_x = N_y = 1024$  for both cases, while the parallel/perpendicular velocity grid is chosen to be  $L_v = 3v_{th,i}$ ,  $L_\mu = 9k_B T_i / B_T$ , with  $32 \times 20$  points in the space  $(v_{\parallel}, \mu)$ .  $\mu$  is the (adiabatic invariant) magnetic moment. In the GK simulations, the initial noise level and spectrum were chosen to match with the corresponding one in the PIC runs. Then, this noise acts as an additional perturbation on top of the one described by Eq. (3).

In the original work by Ref. 11, the guide field  $B_g$  is kept constant for a given set of parameters, while the asymptotic field  $B_{\infty y}$  is reduced to reach the effect of a higher guide field in the PIC runs. Instead of that approach, we choose to keep the total magnetic field  $B_T$  constant while varying the relative guide field strength. This approach allow us to reach the very low guide field regime with the PIC code, and thus to be able to distinguish some phenomena that would not appear otherwise (with the original choice of keeping  $B_g$  constant). Obviously, this choice does not affect significantly the comparison with the GK simulations in the large guide field limit, where convergence is expected.

### III. REPRODUCTION OF PREVIOUS COMPARISON WORK

In this section, we first reproduce the results of the previous comparison work in order to identify the key open problems that will be addressed in this and the upcoming paper.

#### A. Global evolution

Similar to Ref. 11, we obtained a similar global evolution for both low and high beta cases with the PIC code ACRONYM and the GK code GENE, as shown in the time history for the reconnection rate in Fig. 1. Note that reconnection rates are smaller in the high beta case compared to the low beta one, as can be expected from the well known reduced efficiency of magnetic reconnection in high  $\beta$  plasma environments. However, the values are still a substantial fraction of  $(d\Psi/dt)/\dot{\Psi}_N \sim 0.1$ . Therefore, fast magnetic reconnection takes place in both cases, even though the low beta runs are in a regime where there should be no dispersive waves that may explain these rates, according to the two fluid analysis in Ref. 12 (see also Ref. 28). This contradiction was already addressed in Ref. 11 and also other recent works<sup>29-31</sup>. Although there is no a full definitive answer to this controversy yet, all these evidences seem to indicate that fast dispersive waves, such as whistler and kinetic Alfvén waves, seems not to play the essential role to explain fast magnetic reconnection in collisionless plasmas. Since the purpose of this paper is different, we are not going to analyze that issue in this work.

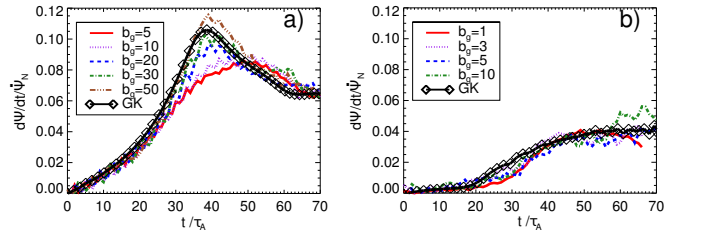


Figure 1. Comparison of reconnection rates  $d\psi/dt$  for the left CS among different PIC guide field cases and the corresponding GK result. This quantity is calculated as the difference in the out-of-plane vector potential  $A_z$  between the X and O points. a) Low beta  $\beta_i = 0.01$  case. b) High beta  $\beta_i = 1.0$  case.

However, some details in the evolution of the system are not exactly the same as in Ref. 11. Although the peak in the reconnection rate is reached more or less at the same time, we observed that the CS is more prone to the development of secondary islands than reported there. They start to appear just after the reconnection peak ( $t \gtrsim 40\tau_A$ ) instead of  $t \gtrsim 75\tau_A$ . We could not find a valid explanation for this. On the other hand, note that in both PIC and GK simulations, the location of the secondary magnetic islands is highly sensitive to the initial noise level, which is random in the PIC runs. Thus, a comparison of the places where these magnetic islands are formed cannot be done between the different PIC and GK runs.

In this point it is worthwhile to mention the speed-up of the GK simulations compared to the PIC runs, the main motivation of using the first numerical method over the second for magnetic reconnection studies. Because of

the choice of keeping the total plasma  $\beta$  constant for different PIC guide fields to properly compare with the GK results, the Alfvén time in units of  $\omega_{pe}^{-1}$  is (practically) linearly proportional to  $b_g$  according to

$$\tau_A \omega_{pe} = \frac{\sqrt{m_i/m_e}}{v_{th,e}/c} \beta_i \frac{L}{\rho_i} \sqrt{1+b_g^2}. \quad (8)$$

In the PIC runs, because the time step has to be proportional to  $\omega_{pe}^{-1}$  for stability reasons, the latter expression will also be proportional to the number of time steps used to reach a given time measured in  $\tau_A$ , and thus to the computational effort. Then, PIC high guide field runs are computationally more expensive than the runs in the low guide field regime (as well as the high beta cases compared to the low beta ones). In fact, for the low beta case, the ACRONYM PIC code used  $3.38 \cdot 10^4$  CPU core-hours to run the cases  $b_g = 5$  up to  $\tau_A = 70$  (the last time shown in Fig. 1), while  $3.33 \cdot 10^5$  CPU core-hours for the case  $b_g = 50$ . On the other hand, the single GENE GK code simulation with which those runs were compared used only 350 CPU core-hours, representing a speed-up by a factor of  $10^3$  when comparing with the largest PIC guide field considered  $b_g = 50$ . This is an additional justification for the importance of a proper comparison study of GK with PIC simulations of guide field reconnection due to these huge computational savings, one of the purposes of the present paper.

All the results and plots to be shown from now on are based in the low beta case. The slightly different conclusions for the high beta case will be briefly analyzed only in the Sec. VI.

## B. Parity/symmetry of magnetic reconnection quantities and linear scaling

For clarity in the terminology that will be used in the rest of this work, we define the parity of all relevant quantities with respect to the  $y$  axis along the CS. A quantity with even/odd symmetry (or symmetric/antisymmetric) will keep/reverse sign under the transformation of coordinates  $(x - L_c) \rightarrow -(x - L_c)$ , where  $L_c = L_x/4, 3L_x/4$  is the location of the left or right CS. This is valid for regions around the separatrices, away from both X and O points.

As indicated by Ref. 11, based in the two fluid analysis by Ref. 32, the thermal pressure and magnetic field fluctuations should display antisymmetric (odd-parity) structures in the separatrices in the strong guide field regime  $b_g \gg 1$ , assuming small fluctuations and asymptotic plasma beta  $\beta_y = 2\mu_0 n_0 k_B T_i / B_{\infty y}^2 \gtrsim 1$  (although a later study<sup>23</sup> showed that this assumption is not necessary for the appearance of an odd-parity magnetic field structure). In addition, both quantities should scale linearly with the magnetic field. For our purposes, it is convenient to specify this term. Indeed, under the same previous assumptions, the fluctuations in thermal pres-

sure are estimated to be (see Eq. 17 of Ref. 32):

$$\frac{\delta P_{th}}{P_{th,0}} \sim \frac{d_i}{l_y} \frac{1}{b_g}. \quad (9)$$

Here,  $P_{th,0} = P_{th}(t=0) = P_0 = 2n_0 k_B T_i$  is the total initial thermal pressure (with contribution of both ions and electrons) and  $l_y$  is the typical length scale of variation of this quantity across the CS, away from the X points, with an order of magnitude  $l_y/d_i \sim \sqrt{\beta_i/2}$ . Similarly, from the pressure equilibrium condition the following estimate for the magnetic fluctuation strength can be derived:

$$\frac{\delta B_z}{B_g} \sim -\frac{\delta P_{th}}{B_g} \sim \frac{d_i}{l_y} \frac{\beta_i}{b_g}. \quad (10)$$

In the rest of this paper we will focus only on this out-of-plane component of the magnetic field, since it is the dominant one for the magnetic pressure in the studied regime. Moreover, since both expressions Eq. (9) and Eq. (10) rely on the pressure equilibrium condition, which involves only the component perpendicular to the magnetic field, the thermal pressure to be used is defined as follows:  $P_{th,\perp} := n_e k_B T_{e,\perp} + n_i k_B T_{i,\perp}$ . For brevity, we will omit the subindex  $\perp$  in the thermal pressure from now on. Note that  $l_y/d_i$  is constant under our normalization for each low/high beta case. Therefore, both fluctuations  $\delta P_{th}$  and  $\delta B_z$  are predicted to scale inversely with the guide field  $b_g$ , providing  $b_g \gg 1$  and assuming the total plasma  $\beta_i$  constant. Note that if we had chosen to keep  $B_{\infty y}$  constant and increase  $B_g$  to have a higher guide field effect, the previous consideration would not be valid and a direct comparison between the different PIC guide field and GK runs would not be possible.

Therefore, the PIC fluctuating quantities will have the same value under the previous assumption if they are multiplied by the factor Eq. (6) proportional to  $b_g$  (in the large guide field limit). The choice of a guide field also fixes the GK ordering parameter  $\epsilon$  Eq. (7). Both factors require the choice of a reference relative guide field,  $b_{g,ref} = 10$  in the low beta case. And because we chose to keep the total magnetic field constant, using Eq. (6) and Eq. (9), the quantity that should be equal among different guide field PIC runs is:

$$\Gamma \delta P_{th} = \frac{\sqrt{1+b_g^2}}{b_{g,ref}} \delta P_{th} = \frac{\sqrt{1+b_g^2}}{10} \delta P_{th}, \quad (11)$$

and analogously for  $\delta B_z$ . For a time shortly after the reconnection peak, this estimate can be seen in Fig. 2 and Fig. 3, respectively. These and all the other figures from the PIC runs shown in this paper, unless stated otherwise, have been averaged over  $t = 0.5\tau_A$  to reduce the effects of the numerical noise.

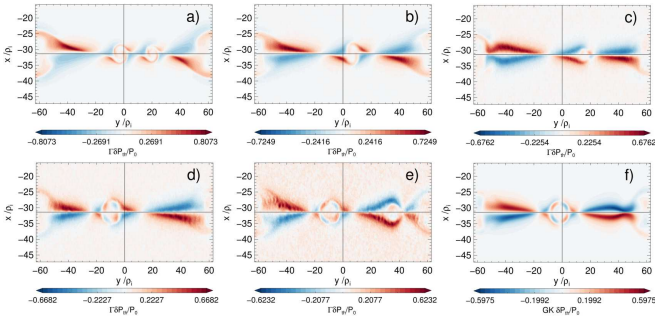


Figure 2. Contour plots of the scaled fluctuations in the (perpendicular) thermal pressure  $\Gamma\delta P_{th}/P_{th,0}$  for different guide fields in the PIC runs and the corresponding GK result, at a time  $t/\tau_A = 50$  shortly after the reconnection peak time. a) PIC  $b_g = 5$ , b) PIC  $b_g = 10$ , c) PIC  $b_g = 20$ , d) PIC  $b_g = 30$ , e) PIC  $b_g = 50$ , f) GK. In the PIC runs,  $\delta P_{th} = P_{th}(t) - 2n_0 k_B T_i$ . The scaling factor  $\Gamma$  (Eq. (6)) for the PIC runs was calculated using a reference guide field  $b_{g,ref} = 10$ . The color scheme is scaled between  $\pm$  the mean plus 3.5 standard deviations of the plotted quantity, a representative maximum as explained in the discussion of Fig. 5.

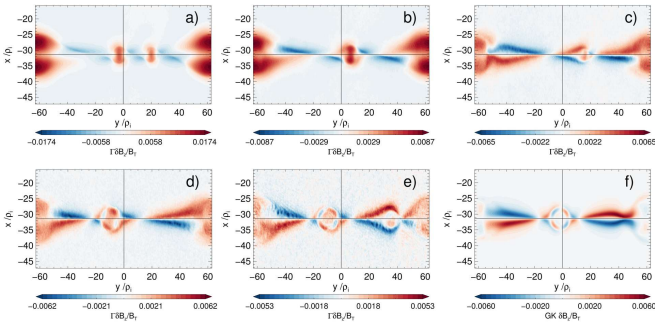


Figure 3. Contours of the scaled fluctuations in the out-of-plane magnetic field  $\Gamma\delta B_z/B_T$  for different guide fields in the PIC runs and the corresponding GK result, at the same time  $t = 50\tau_A$  as shown in Fig. 2. a) PIC  $b_g = 5$ , b) PIC  $b_g = 10$ , c) PIC  $b_g = 20$ , d) PIC  $b_g = 30$ , e) PIC  $b_g = 50$ , f) GK. In the PIC runs,  $\delta B_z = B_z(t) - B_z(t = 0)$ , where the initial  $B_z(t = 0) \approx B_g$  for large enough guide field according to Eq. (2). The scaling factor  $\Gamma$  is the same used in Fig. 2. The color scheme is calculated using the same method described in Fig. 2.

From Figs. 2 and 3 we can infer the same expected result from the previously sketched two fluid model<sup>32</sup>: the convergence of the PIC results towards the GK ones in the limit of strong guide field, in both odd symmetry and scaling to the guide field. This was already confirmed by Ref. 11 in the region close to the separatrices, where that model holds. However, we can immediately notice that not only the symmetry between both separatrices is broken in the low guide field regime, but also the appearance of an additional magnetic field in the secondary magnetic islands not visible in GK or the strong PIC guide field regimes. In this paper we will focus in these differences. For brevity, other differences between PIC/GK will be

addressed in a follow-up paper.

It is important to mention at this point that the PIC runs in the high guide field regime are much more affected by numerical noise than in the low guide field regime. This is because, in our setup,  $B_{\infty y}$  decreases for increasing  $b_g$ . Then, for large guide fields the signal-to-noise ratio can be very low, as can be seen in the extreme case  $b_g = 50$  in Fig. 2(e) and Fig. 3(e) (even with the extended temporal average). Therefore, although in principle there is no limitation due to numerical constrains on the electron gyromotion for even higher guide fields (in our setup,  $\rho_e$  and  $\Omega_{ce}$  are constant for different guide fields), the PIC results in this regime will not be reliable due to this unfortunate fact.

#### IV. CORE MAGNETIC FIELD AND PRESSURE EQUILIBRIUM CONDITION

The core magnetic field in the secondary magnetic islands, as well as in the  $y$  boundaries, can be understood from several points of view. In this section, we will describe it in the framework of deviations from the two fluid model sketched in the previous Sec. III B, based on the pressure equilibrium condition.

##### A. Numerical reason for core magnetic field and pressure equilibrium condition

First of all, why is a magnetic field in the secondary magnetic islands (in the PIC low guide field regime) as well as in the  $y$  boundaries allowed and not compensated by a decrease in the thermal pressure? Obviously, this has to do with violations of the pressure equilibrium condition. In the GK code, the sum of magnetic field pressure and perpendicular thermal pressure is kept identically equal to zero (to machine precision). On the other hand, PIC codes may allow large deviations from the pressure equilibrium condition for finite guide fields. Let us quantify this by combining Eq. (9) with Eq. (10), relating thus the fluctuations in magnetic and (perpendicular) thermal pressures:

$$\frac{\delta B_z}{B_g} = -\beta_i \frac{\delta P_{th}}{P_{th,0}}. \quad (12)$$

The respective 2D (frequency) histograms with the correlation of the left and right hand side of Eq. (12) are shown in Fig. 4(middle row) for different guide fields, at the same point in time that is shown in Fig. 2 and Fig. 3. These plots were generated by selecting the interesting region close enough to the center of the CS, in order to eliminate as much as possible any fluctuation in the almost unperturbed region away from the CS (not involved in the reconnection process). The chosen region contains all the points with a current density  $J_z$  above 10% of its initial peak value (see Fig. 4(top row)). In order to

show the locations of deviations in the pressure equilibrium condition, we also plot in Fig. 4(bottom row) the corresponding fluctuations in the total pressure,

$$\frac{\delta P_{\text{total}}}{P_{\text{th},0}} = \frac{P_{\text{th}} + P_{\text{mag}}}{P_{\text{th},0}} - 1 - \frac{1}{2\beta_i}, \quad (13)$$

with  $P_{\text{mag}} = B^2/(2\mu_0)$ .

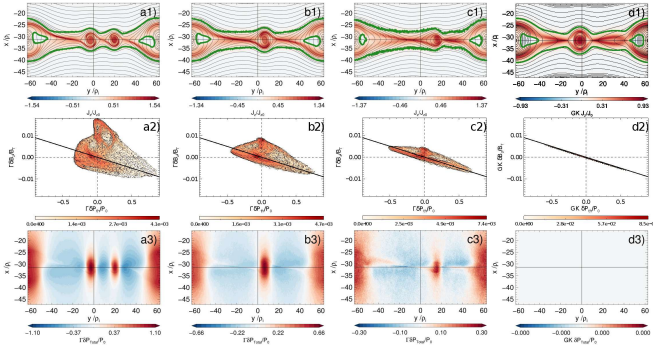


Figure 4. Top row. Contour plots of the out-of-plane current density  $J_z/J_z(t=0)$  for different PIC guide fields and the corresponding GK result, at a time  $t/\tau_A = 50$ . a1) PIC  $b_g = 5$ , b1) PIC  $b_g = 10$ , c1) PIC  $b_g = 20$ , d1) GK. Magnetic field lines are shown in black contour lines. Note that because Eq. (5),  $J_z(t=0) = J_{zN} \cdot J_N$  varies with the PIC guide field (through  $J_N$ ). The region inside the green contour corresponds to values of  $J_z$  higher than 10% of the initial value  $J_z(t=0)$ .

Middle row: Respective 2D (frequency) histograms with the correlation between the magnetic and thermal fluctuations  $\Gamma\delta B_z/B_T$  and  $\Gamma\delta P_{\text{th}}/P_{\text{th},0}$  for the same runs and time as above. a2) PIC  $b_g = 5$ , b2) PIC  $b_g = 10$ , c2) PIC  $b_g = 20$ , d2) GK. The points used to generate these plots correspond to those located inside of the green contour in the plots for  $J_z$  in the first row. The diagonal black straight line with slope  $-\beta_i$  represents the pressure equilibrium condition in the limit of strong guide field Eq. (12).

Bottom row: Respective contour plots for the scaled total pressure  $\Gamma\delta P_{\text{total}}/P_{\text{th},0}$ . a3) PIC  $b_g = 5$ , b3) PIC  $b_g = 10$ , c3) PIC  $b_g = 20$ . d3) GK. The latter is identically zero to machine precision.

An ideal pressure equilibrium in this limit, given by Eq. (12), should follow a straight line with slope  $-\beta_i$  (black diagonal line in the middle row of Fig. 4). Then, the numerical reason of the observed deviations in the PIC low guide field regime is a consequence of the large violations of this pressure equilibrium condition. In the middle row of Fig. 4, most of the points are along the line  $-\beta$  for a guide field  $b_g = 20$ , with an increasing spread in the lower guide field regime. The corresponding GK results follow very accurately that line. Note a distinctive “bump” in the region  $\delta P_{\text{th}} \sim 0$  with  $\delta B_z \gtrsim 0$  (upper part), which is very noticeably for a PIC guide field  $b_g = 5$ . There, the strong magnetic fluctuations are not compensated by a drop in the thermal pressure. We can see in the corresponding plots of the fluctuations in the total pressure  $\delta P_{\text{total}}$  (Fig. 4(bottom row))

that these regions are mostly in the secondary magnetic islands and in the  $y$  boundaries. This excess of total pressure generates a net force towards the exterior of the magnetic islands, leading to an expansion in reconnection time scales ( $\sim \tau_A$ ). Note that the  $\delta P_{\text{total}}$  increases going to the lower guide field regime, even though this quantity has been scaled linearly to the guide field. That is to be expected, since the maximum level of fluctuations for this time are of the order of the initial equilibrium values, and the assumption on which Eq. 12 is based (small fluctuations, the same one used in GK) breaks down. For times after the reconnection peak, when secondary islands are active, we could observe that  $\delta P_{\text{total}}$  actually scales quadratically with the guide field. This means that  $\Gamma^2 \delta P_{\text{total}}/P_{\text{th},0}$  shows the same fluctuation level for different guide fields.

In the 2D histograms of Fig. 4(top row) it is also possible to discern an asymmetric distribution along the straight line of the pressure equilibrium condition that is more important in the PIC low guide field regime: there are more points located in the right bottom quadrant ( $\delta P_{\text{th}} > 0$  and  $\delta B_z < 0$ ) than in the left upper quadrant ( $\delta P_{\text{th}} < 0$  and  $\delta B_z > 0$ ). The corresponding GK results show a symmetric behaviour (See also Fig. 2). This is an indication of the asymmetry in the separatrices for the PIC low guide field regime: the maximum values of  $\delta P_{\text{th}}$  are larger than the absolute value of the minimum ones in each pair of separatrices.  $\delta B_z$  displays similar behaviour but to a much smaller extent. We will explain the reasons in Sec. V A.

Another important observation in the middle row of Fig. 4 is the presence of a set of points in a straight line parallel to the pressure equilibrium line, but shifted upwards. We checked that they are located in the regions with enhanced current density: both the pair of separatrices with enhanced number density (especially far away from the X point) and the “S” shape inside of the secondary magnetic islands. These regions contributes to further deviations in the pressure equilibrium condition in both  $\delta P_{\text{th}}$  and  $\delta B_z$ .

Therefore, although the magnetic field fluctuations  $\delta B_z$  predicted by the GK simulations can be comparable to the PIC ones in the low guide field regime ( $b_g = 5, 10$ ) close to the separatrices, this is not true inside of the secondary magnetic islands or the periodic  $y$  boundaries. That phenomenon can be understood because of the larger deviations from the pressure equilibrium condition generated by an uncompensated additional magnetic pressure, significant only in the PIC low guide field regime.

## B. Time evolution of deviations in the pressure equilibrium condition

A convergence study focusing in one single time, like the one shown in the previous Figs. 2 and 3 may be misleading. Furthermore, as we already showed, even though

the reconnection rates may take similar values for a given time, the evolution of the physical quantities associated with the reconnection process is very different. That is why in this section we analyze the time evolution of the quantities related to the pressure equilibrium between both codes. Thus, we can detect from what time the previously described core magnetic field, and the associated deviations in the pressure equilibrium condition, start to appear. This also complements the work of Ref. 11, since in that comparison work the time evolution of the quantities related with reconnection was not investigated.

Now, in order to make quantitative estimations, we chose to track the maximum of  $\delta P_{th}$  and  $\delta B_z$  in a region centered in the left CS (same area shown in Fig. 2 and 3). For the PIC simulations, in order to decrease the effects of the numerical noise, we chose the maximum value of the previous quantities as equal to the mean plus 3.5 standard deviations. We do not consider the absolute maximum because is very prone to outlier values, especially in the PIC high guide field regime. In addition, the initial value of the respective fluctuating quantity is subtracted, since it mostly measures the numerical PIC noise, being enhanced for higher guide fields. Moreover, the scaling given by the estimates Eq. (9) and Eq. (10) requires an initial zero offset in order to have a proper comparison with the corresponding GK results. The results are shown in Fig. 5.

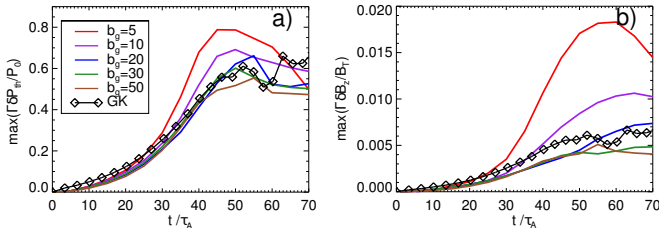


Figure 5. Time history of the maximum value of the scaled thermal pressure  $\Gamma\delta P_{th}/P_{th,0}$  (a) and magnetic fluctuations  $\Gamma\delta B_z/B_T$  (b) for different PIC guide field cases and the corresponding GK result. In the PIC runs, the “maximum” is defined as equal to the mean plus 3.5 standard deviations of the respective quantities, consistent with the color scheme used in Figs. 2 and 3. In addition, the initial value of the respective fluctuating quantities is subtracted in the PIC results. As explained in the main text, these methods are for reducing the effects of the numerical PIC noise as much as possible.

First of all, we can note in Fig. 5 that the maximum of the thermal fluctuations is reached around  $t \sim 50\tau_A$  for all the cases, after the reconnection peak time  $t \sim 40\tau_A$  when also the secondary magnetic islands start to form. The magnetic fluctuations reach maximum values even later. This is an indication of an additional process generating  $\delta B_z$ , different from the Hall term due to the reconnection process itself (close to the X point, in the separatrices). It is driven by physical processes deeply in the non-linear phase of magnetic reconnection, not being

straightforward to describe them as an steady process. This is also the justification for showing these quantities at a time  $t = 50\tau_A$  in Figs 2 and 3.

In Figs. 5(a)-(b) we can see that the time evolution of both maximum  $\Gamma\delta P_{th}$  and  $\Gamma\delta B_z$  shows a convergence among the PIC runs in the strong guide field limit, i.e.: the respective curves get closer and closer for all guide fields  $b_g \gtrsim 20$ . As can be expected, the GK values follow a similar trend as the strongest PIC guide field ( $b_g = 50$ ). As it was pointed out by Ref. 11, this agreement extends to many other particle related quantities (densities, temperatures, outflow speeds). However, there are important deviations for smaller values of the PIC guide field  $b_g$ . These deviations start to be noticeably for earlier times for lower values of  $b_g$ . For example, the PIC run  $b_g = 5$  shows deviation from the GK curve of  $\Gamma\delta B_z$  already in  $t \gtrsim 20\tau_A$ , while  $b_g = 30$  only after  $t \gtrsim 45\tau_A$ . Note that deviations in  $\Gamma\delta P_{th}$  are smaller than those of  $\Gamma\delta B_z$ .

The physical reasons of the differences in the PIC runs for  $\Gamma\delta P_{th}$  as shown in Fig. 5(a) will be addressed in the follow-up paper (they have to do with the different contributions of electrons and ions to the specific components of the pressure tensor, as well as non-thermal features of the electron distribution function). Here we explain and analyze with much more detail the differences regarding the magnetic fluctuations  $\Gamma\delta B_z$  shown in Fig. 5(b).

Although useful, Fig. 5 cannot provide us with information about the relation of these maxima with the pressure equilibrium condition (i.e.: the location in the space of thermal  $\delta P_{th}$  and magnetic  $\delta B_z$  fluctuations). For that purpose, in Fig. 6 we show the 2D histograms relating these fluctuations, for three characteristic times in the evolution of the lowest PIC guide field run  $b_g = 5$ .

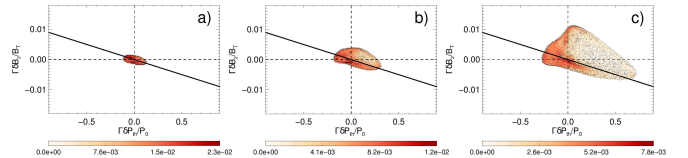


Figure 6. 2D (frequency) histograms with the correlation between the scaled thermal and magnetic fluctuations  $\Gamma\delta B_z/B_T$  and  $\Gamma\delta P_{th}/P_{th,0}$ , for three characteristic times in the evolution of a low enough PIC guide field run  $b_g = 5$ . a)  $t = 20\tau_A$ , b)  $t = 30\tau_A$ , c)  $t = 40\tau_A$ . Similarly to Fig. 4, the points used to generate these plots correspond to the regions with the current density  $J_z$  above the 10% of its initial value  $J_z(t = 0)$ . The diagonal black straight line with slope  $-\beta_i$  represents the pressure equilibrium condition in the limit of strong guide field Eq. (12).

We can see in Fig. 6 that the asymmetry along the pressure equilibrium line located in the right bottom part ( $\delta P_{th} > 0$  with  $\delta B_z < 0$ ) starts from the very beginning ( $t = 20\tau_A$ ), indicating the high values of thermal pressure are generated via a process that is active since the start. The points tracked in Fig. 6(a) are mostly located in this region corresponding to the separatrices. On the other hand, the “bump”  $\delta P_{th} \sim 0$  with  $\delta B_z \gtrsim 0$  (indicating

violation of the pressure equilibrium condition) starts to develop just before of the reconnection peak time ( $t \sim 30\tau_A$ , Fig. 6(b)). These points are located inside of the secondary magnetic islands or the  $y$  boundaries. This is an indication of being caused via a process that needs to be build up during the evolution of reconnection. Later, in Fig. 6(c) for  $t \sim 40\tau_A$ , the points spread even further in the “bump region”, indicating the shift of the largest deviations of the pressure equilibrium condition from the separatrices to the “bump”. The physical origin of this phenomenon will be explained in the following Sec. V.

We can summarize this section by saying that PIC and GK simulations predict similar evolution for both magnetic and thermal pressures especially during the linear phase of reconnection. The formation of secondary magnetic islands breaks this similarity, producing deviations especially in the magnetic fluctuations  $\delta B_z$ , that reach maxima for times much later than the reconnection peak time.

## V. CORE MAGNETIC FIELD AND SHEAR FLOW

In this section we describe the physical mechanism that leads to the generation of core magnetic field in the PIC low guide field simulations, as a result of a necessarily slightly different initialization in comparison with the GK runs, thus complementing the previous Sec. IV. In this point, it is important to mention some previous works that have found this feature, such as Ref. 20. They reported the generation of core magnetic field during the coalescence of secondary magnetic islands, as result of a Hall effect that twists magnetic field lines, plus flux transport with the associated pile up of the out-of-plane magnetic field. In our case, the mechanism is more related to the first one but due to a different reason.

### A. Initial shear flow

The mechanism responsible for the generation of the core magnetic field seen in the PIC low guide field runs (see, e.g., Figs. 3(a)-(b)) is due to the development of strong in-plane currents. Initially, the PIC runs have, in addition to the out-of-plane component  $J_z$  that sustains the asymptotic magnetic field (analogous to the Harris equilibrium), an in-plane component of the electron current density  $J_y$ , in order to satisfy the force free condition and the Ampère’s equation. It is given by:

$$J_{e,y} = \frac{B_{\infty y}}{\mu_0 L} \frac{\left[ \frac{\tanh(\frac{x-L_x/4}{L})}{\cosh^2(\frac{x-L_x/4}{L})} + \frac{\tanh(\frac{x-3L_x/4}{L})}{\cosh^2(\frac{x-3L_x/4}{L})} \right]}{\sqrt{b_g^2 + \cosh^{-2}(\frac{x-L_x/4}{L}) + \cosh^{-2}(\frac{x-3L_x/4}{L})}}. \quad (14)$$

This represents a counterstreaming flow of electrons with respect to the central line of each CS (see Fig. 7(b)). The maximum of  $V_{e,y} = J_y/(en_0)$  (no contribution from the

initially stationary ions) decreases asymptotically for increasing guide fields (consequence of a decreasing  $B_{\infty y}$ ), as can be seen in Fig. 7(a). Equivalently: the value of the total kinetic energy of the shear flow, the source of free energy, is higher in the low guide field regime, with a strong dependence on this parameter (approximately,  $\propto 1/b_g^4$ ). Therefore, it converges very quickly to the GK initialization, where this initial electron shear flow is absent (zero kinetic energy of the shear flow).

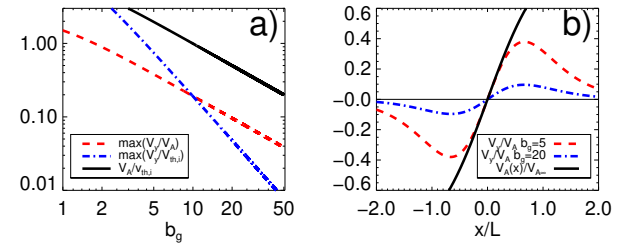


Figure 7. a) Maximum initial value of the in-plane electron flow speed  $V_{e,y}$  on dependence on the guide field  $b_g$ , normalized to the in-plane Alfvén speed  $V_A$  and to the constant  $v_{th,i}$ . The ratio of both normalization factors,  $V_A/v_{th,i}$ , is shown in black continuous line. Note that both axis are in logarithmic scale.

b) Initial profiles of in-plane electron flow speed  $V_{e,y}(x)/V_A$  across a CS centered in  $x = 0$  for two values of guide field. The initial in-plane local Alfvén speed  $V_A(x)$  is shown in black continuous line.

From Fig. 7(a) we can infer an important conclusion based on the relative ratio of the Alfvén to ion thermal speed. Due to the choice of keeping the total plasma  $\beta$  constant to properly compare with GK simulations, the PIC runs will invariably have to change this parameter for different guide fields:

$$\frac{V_A}{v_{th,i}} = \frac{1}{\sqrt{1+b_g^2}} \frac{1}{\sqrt{\beta_i}}. \quad (15)$$

Note that  $v_{th,i}$  is constant for different guide fields, while  $V_A$  scales inversely with it. This means that the ratio  $V_A/v_{th,i}$  increases for lower PIC guide fields: from  $V_A/v_{th,i} = 0.2 \rightarrow 1.96$  going from  $b_g = 50 \rightarrow 5$  in this low beta case. This value plays an essential role in the GK simulations, because of the perpendicular drift approximation. This is the assumption that the perpendicular velocities  $\vec{V}_{\perp}$  are caused only by the  $\vec{E} \times \vec{B}$ , diamagnetic  $\nabla P_e$  and other similar drifts. The perpendicular approximation breaks down when the in-plane speeds are close to the ion thermal speeds, such as the typically obtained in magnetic reconnection outflows when  $V_A \sim v_{th,i}$ . Therefore, deviations from the real physical behaviour of a Vlasov plasma modeled via PIC simulations are expected in the GK approach when the ratio  $V_A/v_{th,i} \sim 1$ . This is precisely the situation when comparing the GK simulations to PIC runs with  $b_g = 5$  or

$b_g = 10$  (the latter is the critical guide field for which  $V_A/v_{th,i} \approx 1$ ).

The initial shear flow is also the responsible for the asymmetric separatrices (see discussion of Fig. 4), especially regarding the preferential  $\delta P_{th} > 0$  over  $\delta P_{th} < 0$ . This behaviour was already pointed out by Ref. 33, where it was attributed to the dynamic pressure of the shear flow, which can tilt the outflow in its incoming direction. As a result, more electrons are piled up preferentially in one pair of the separatrices over the other one for sufficiently low PIC guide fields, contributing to the increase of density, temperature and thermal pressure (see Fig. 2). This is a behaviour not predicted by the two fluid model sketched in Sec. III B, since it was developed without these initial flows. An extended discussion about this topic will be given in the follow-up paper.

It is important to mention that the “S” shape of  $\delta B_z$  in the secondary magnetic islands is not directly related to the asymmetry induced by the shear flow. This has been observed in previous hybrid simulations such as in Ref. 19, where it was attributed to an ubiquitous feature of guide field reconnection (such as Harris sheets without initial shear flow), due to the asymmetric shift of the outflows from the X points in comparison with anti-parallel reconnection. However, that study was carried out in the regime of guide fields even smaller than the reconnected magnetic field ( $b_g < 1$ ), and therefore the conclusion might not be applied directly to our case.

## B. Current/flows in secondary magnetic islands

As a result of the initial shear flow, PIC runs with sufficiently low guide field build up a net vortical current as the reconnection process goes on, inside of the secondary magnetic islands and the periodic  $y$  boundaries, as can be seen in Fig. 8. The formation of secondary magnetic islands wraps up magnetic field lines around them, deflecting the electron shear flow in the same direction. Therefore, a net out-of-plane magnetic field is generated (See Fig. 3). Note that the direction of the curl of  $\vec{J}$  coincides with the direction of the out-of-plane magnetic field ( $+z$  direction points into the page). As expected, there is a working dynamo process in these places, i.e.:  $\vec{J} \cdot \vec{E} < 0$ , involving a transfer of energy from the bulk electron motion to the magnetic field. High guide field PIC or GK runs do not show this effect (negative values of  $\vec{J} \cdot \vec{E}$  are seen only near the outflows, due to the bulk motion of the plasma). A comparison of this process to the dissipation  $\vec{J} \cdot \vec{E} > 0$  close to the X points will be given in the follow-up paper.

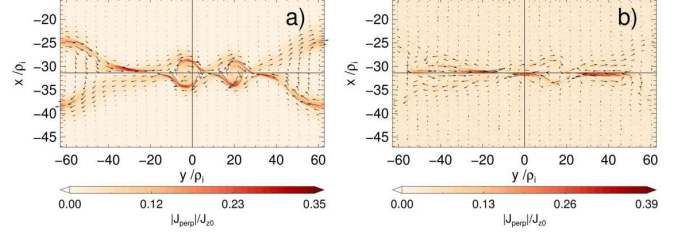


Figure 8. Vector plot of the in-plane current  $\vec{J}_{\perp} = J_x \hat{x} + J_y \hat{y}$  for two cases of PIC guide fields a)  $b_g = 5$  and b)  $b_g = 20$ , at a time  $t = 50 T_A$ . Color coded is the magnitude of this in-plane current  $|J_{\perp}|/J_z(t = 0)$ . Note that because Eq. (5),  $J_z(t = 0) = J_{zN} \cdot J_N$  varies with the PIC guide field (through  $J_N$ ).

It is interesting to mention that the tilting of magnetic islands and generation of concentric vortical flows inside of them as result of shear flows has been seen in both 2D MHD and Hall-MHD simulations (see Ref. 34 and references therein). These effects were seen for shear flows in sub-Alfvénic regime, in agreement with our parameter regime (see Eq. (7) and Fig. 7). Note that the structure of the core magnetic field becomes more symmetric inside of the secondary magnetic islands in the PIC low guide field regime than the GK or PIC high guide field regime (see Fig. 3). This is in agreement with Ref. 23, who carried out a two fluid analysis of collisionless tearing mode under the influence of a shear flow. By taking into account electron inertia, they showed that the generated out-of-plane magnetic field can exhibit a significant symmetric structure for low  $\beta_y < 1$  (in our case, for PIC  $b_g = 5$ ,  $\beta_y \approx 0.52$ ), in opposition to the characteristic antisymmetric or quadrupolar structure of  $\delta B_z$  for  $\beta_y \gg 1$  (in our case, for PIC  $b_g = 50$ ,  $\beta_y \approx 50$ ).

The current inside of the magnetic islands, significant only in the low guide field regime, is produced due to a Hall effect: a decoupling of motion between electrons and ions, as shown in Fig. 9 for two PIC guide field cases and the corresponding GK result. For the lowest PIC guide field run  $b_g = 5$ , the ions follow the outflow due to reconnection from the X point (Fig. 9(b1)), but the electrons keep their initial shear flow and are only weakly deflected (Fig. 9(a1)) by that reconnection outflow, following a vortical flow pattern inside of the magnetic islands. This characteristic flow pattern is barely visible for a higher guide field of  $b_g = 20$  (see Figs. 9(a2)-(b2)) and totally absent for the GK run (see Figs. 9(a3)-(b3))

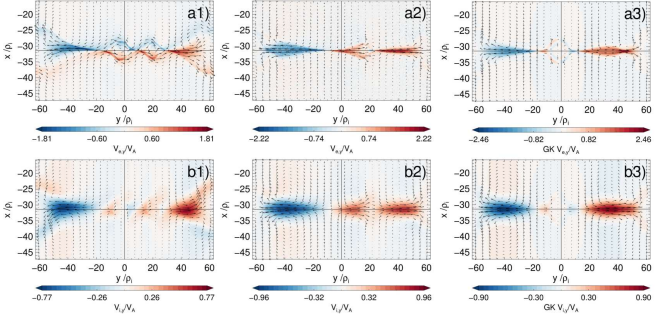


Figure 9. Top row: Vector plot of the in-plane electron bulk velocity for different PIC guide fields and the corresponding GK result, at a time  $t = 50\tau_A$ . Color coded is the  $V_{e,y}/V_A$  component. a1) PIC  $b_g = 5$ , a2) PIC  $b_g = 20$ , a3) GK. Bottom row: Same as above but for the in-plane ion bulk velocity  $V_{i,y}/V_A$ . b1) PIC  $b_g = 5$ , b2) PIC  $b_g = 20$ , b3) GK.

It is important to mention that because the generation of magnetic field is due to a Hall effect, their effects will be stronger when the CS is much thinner than  $d_i$ <sup>35</sup>, which applies very well to our case ( $L = 0.2d_i$ ). Therefore, in thicker CS these effects should be significantly reduced and an agreement between PIC and GK simulations of magnetic reconnection will be more easily reached.

The speed of the electron outflows from the main X point due to reconnection is a few times the asymptotic Alfvén speed  $V_{e,y} \sim 1.8V_A$ . It varies weakly with the guide field in the PIC runs. On the other hand, the ion outflow speeds only reach sub-Alfvénic values  $V_{e,y} \sim 0.8V_A$ , and are much more constant among different PIC guide fields and the GK runs. This is, to a first order, in good agreement with the standard two fluid theory of magnetic reconnection by Ref. 36: the outflow speeds from the X point are of the order of the in-plane Alfvén speed  $V_A$  for ions and in-plane electron Alfvén speed  $V_{Ae} = \sqrt{m_i/m_e}V_A$  for electrons. But the initial shear flow is of course strongly dependent on the guide field (See Fig. 7). The combination of both effects determines the critical PIC guide field for which the shear flow can generate the current that builds up the core magnetic field ( $b_g \lesssim 20$ ).

In Fig. 9 we can also note another important difference between the secondary magnetic islands for different PIC guide field regimes. For  $b_g = 5$ , the electron outflow from the secondary X points close to these islands is strong enough to be noticed over the dominant outflow from the main X point (See Fig. 9(a1)). On the other hand, for higher guide field such as  $b_g = 20$ , the electron outflow speed from the secondary magnetic islands is reduced to such extent that cannot overcome the reconnection outflow from the main X point and it is simply carried away from this (Fig. 9(a2)). As it can be expected, this behaviour is also seen in the GK simulations (Fig. 9(a3)). Therefore, although the secondary magnetic islands are formed for all guide field regimes in the PIC runs and also in GK simulations, displaying a similar morphology, they have essentially different properties. The dominance of

the main X point is much more significant for the PIC low guide field regime than in the high guide field one or the GK runs, a behaviour that can only be captured by PIC simulations.

### C. Time evolution of electron/ion flows: influence of initial shear flow

Now, let us investigate how these currents are build up from the initial one in the PIC runs with sufficiently low guide field. First, in order to distinguish the relative contributions of the initial shear flow and the reconnection outflows, it is convenient to analyze the system for earlier times, during the linear phase of tearing mode growth, when there are no secondary magnetic islands. This can be seen in Fig. 10, where we compare the full electron outflow and the one obtained by subtracting the initial shear flow.

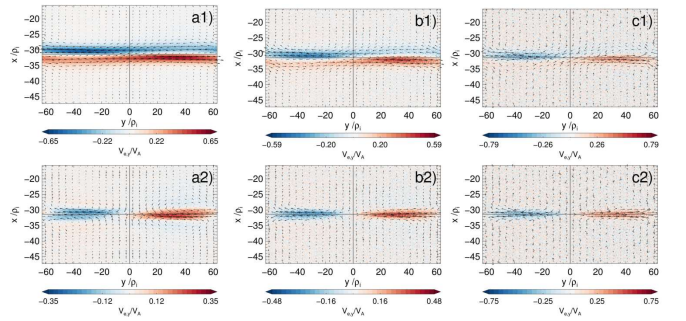


Figure 10. Top row: Vector plots of the in-plane electron bulk velocity for different PIC guide fields, at a time  $t = 20\tau_A$ , early in the linear phase of reconnection. Color coded is the  $V_{e,y}/V_A$  component. a1) PIC  $b_g = 5$ , b1) PIC  $b_g = 10$ , c1) PIC  $b_g = 20$ . Bottom row: Same vector plots as above, but with the initial shear flow subtracted:  $(V_{e,y} - V_{e,y}(t = 0))/V_A$ . This gives the outflow due to reconnection. a2) PIC  $b_g = 5$ , b2) PIC  $b_g = 10$ , c2) PIC  $b_g = 20$ .

In Fig. 10(a1) and Fig. 10(a2), the electron flow is dominated by the initial shear flow for this case of smallest guide field  $b_g = 5$ : the reconnection outflow is very weak to produce any appreciable effect. This can be measured through the maximum values: the total flow speed reaches  $V_y \sim 0.65V_A$ , while the reconnection outflow speed reaches  $V_y \sim 0.35V_A$ . On the opposite case, for a stronger guide field of  $b_g = 20$  (Fig. 10(c1) and Fig. 10(c2)), the shear flow is weak enough that the overall electron flow mostly follows the reconnection one, being only weakly deflected (total flow speed reaches  $V_y \sim 0.79V_A$ , while the reconnection outflow speed reaches  $V_y \sim 0.75V_A$ ). For later times, the dynamics is dominated by the reconnection outflow in both cases, in such a way that  $V_{e,y} \gg V_{e,y}(t = 0)$  (see Fig. 9). Note that the reconnection outflows are always symmetric (even), while the odd parity of the shear flow with

respect to the center of the CS breaks this symmetry, as we already explained in Sec. V A.

We checked that the electron and ion inflow/outflow speeds have similar values among different PIC guide field and GK simulations when measured in units of the Alfvén speed for different times (see, e.g., Fig. 9). The agreement, as can be expected, is better in the linear phase of reconnection. As a result, the in-plane current  $\vec{J}_\perp$  (proportional to  $\vec{V}_{i,\perp} - \vec{V}_{e,\perp}$ ) will also display similar values among different PIC guide fields when the same normalization is used (see Fig. 8). But the generation of the magnetic field  $B_z$  depends on  $J_\perp$  measured in absolute units (without normalization to  $J_N$ ). The initial value of the unnormalized current does change with the guide field due to the relative ratio of Alfvén to thermal speeds Eq. (15). Furthermore, the generation of magnetic field  $\delta B_z$  can be estimated as follows, by using the Ampère's law, neglecting displacement current and approximating the curl  $\nabla \times \vec{B}$  by the gradient scale length  $1/\Delta L$ :

$$\frac{\delta B_z}{B_g} \approx \frac{\Delta L}{\rho_i} \left( \frac{\mu_0 \rho_i}{B_g} \right) J_\perp. \quad (16)$$

Defining the constant  $\Lambda = \mu_0 \rho_i / B_g$ , we infer that  $\delta B_z / B_g$  in absolute units ( $B_g$  is constant for different PIC guide fields) is on the order of  $\Lambda J_\perp$  when the length scale of the magnetic field is on the order of  $\rho_i$ , not dependent on the guide field. In our runs,  $\Delta L$  can be estimated as the size across the  $x$  direction of either the secondary magnetic islands close to the  $X$  point ( $\sim 10\rho_i$ ), or the magnetic island at the  $y$  boundaries ( $\sim 18\rho_i$ ). Thus, the time history of the maximum value of both components of  $\Lambda = J_\perp$  is shown in Fig. 11.

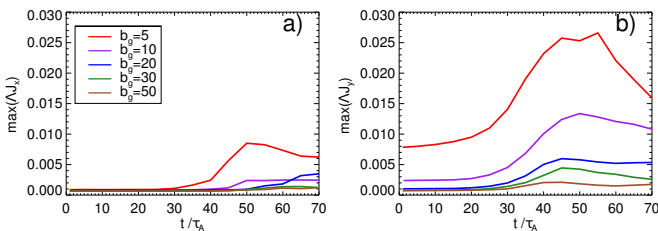


Figure 11. Time history of the maximum value of the fluctuations on the in-plane current density for different PIC guide fields cases. a)  $\Lambda J_x$ . b)  $\Lambda J_y$ . Note that this quantity does not have a normalization factor dependent on the guide field as Fig. 8 (it is measured in absolute units). These values have to be compared with the ones for  $\delta B_z / B_g$  shown in Fig. 5.

Fig. 11(b) shows the presence of the initial current density  $J_y$  which is increasingly important for lower PIC guide fields. Both in-plane components  $J_x$  and  $J_y$  start to grow after the reconnection peak time. Nevertheless, most of the contributions to the total in-plane current come from the  $J_y$  component (compare with Fig. 11(a)). There is a good agreement (in the order of magnitude) of the maximum values that  $\Lambda J_y$  reach with the corresponding maximum values of  $\delta B_z$  (see Fig. 5(b)) for different

guide fields. Note that the factor  $\Gamma$  should be removed in the latter for a proper comparison (e.g., for  $b_g = 5$ , the maximum is  $\delta B_z / B_g \sim 0.034$ ). It is also important to remark that the maximum values of  $J_y$  are reached in the boundaries of the locations where  $\delta B_z$  peaks: around the secondary magnetic islands and the  $y$  boundaries (neglecting the region in the separatrices with almost zero curl). The most important conclusion that can be inferred from Fig. 11 is that the maximum values of  $J_y$ , and so  $\delta B_z$ , become negligible in the PIC higher guide field limit when measured in absolute units. Therefore, magnetic field generation is only effective in the lower PIC guide field regime.

All these are indications that the generation of the core magnetic field  $\delta B_z$  is due to a process that evolves with the formation of magnetic islands and becomes increasingly important for lower PIC guide fields, and that is why it should not be taken into account when comparing PIC with GK simulations of magnetic reconnection.

#### D. Boundary effects in core magnetic field generation

We already mentioned that in the PIC low guide regime, besides of the secondary magnetic islands, a core magnetic field is also generated in the  $y$  boundaries. This is mostly due to numerical reasons, resulting from the colliding outflows from reconnection in the main  $X$  point and the periodic boundary conditions (equivalent to a configuration with multiple  $X$  points). Reconnection in the PIC low guide field regime produces faster electron outflows in absolute units, since they have approximate similar values in units of  $V_A$ , but this scales as  $\propto 1/b_g$ . Therefore, this process could be avoided by choosing longer boxes, as it has been pointed out by Ref. 19. Note that the main secondary island in the  $O$  point of this CS (due to the initial perturbation), is located in this same place ( $y$  boundaries), generating a magnetic field via the same process described before for the secondary magnetic islands. Thus, the total magnetic field in these locations has contributions of both physical and boundary effects.

#### E. Influence of shear flow in reconnection

Now, let us focus on the effects of the shear flow and associated magnetic field generation in reconnection. As we can see in Fig. 1, the reconnection rates are smaller for the lower guide field cases  $b_g = 5, 10$  compared with the high guide field regime or the GK runs. This can be understood in terms of three different reasons. First, the outflows from the  $X$  points should be less efficient (slower) because of the additional magnetic pressure due to the core  $\delta B_z$  in the secondary magnetic islands (and  $y$  boundaries). This process tends to inhibit the CS thinning. Note that this additional out-of-plane magnetic field has higher relative importance with respect to the guide field precisely in cases with low PIC guide field

(See, e.g., Fig. 5). Second, as indicated by Ref. 33, the magnetic tension in the reconnected magnetic field lines should be released by the shear flow, reducing the outflow speed produced by them and thus decreasing reconnection rates. This was also confirmed by a kinetic dispersion relation and 2D PIC simulations for thin CS<sup>22</sup>. And third, part of the available magnetic energy for reconnection that should be converted into particle energy is given back when the Hall currents are formed in the secondary magnetic islands. Overall, it is clear that reconnection rates should be reduced in the PIC low guide field regime, if the total plasma  $\beta$  is kept constant.

It is important to mention that Ref. 33 analyzed the effects of an in-plane shear flow in magnetic reconnection under a Hall-MHD model (without guide field). They concluded that reconnection rates should be reduced in presence of a shear flow according to the scaling law  $\psi_s = \psi(1 - V_0^2/V_A^2)$ , where  $V_0$  is the initial flow speed,  $\psi$  and  $\psi_s$  reconnection rates without and with shear flow, respectively. As we can see in Fig. 7, the extra factor  $1 - V_0^2/V_A^2$  is non-negligible in the lower PIC guide field regime  $b_g = 5, 10$  (with factors 0.57 and 0.89, respectively). For the corresponding PIC runs, the measured reduction in reconnection rates is on the order of 20% compared to the GK results (see Fig. 1), equivalent to a factor of 0.8. Note that although the estimate should not be applied directly to our case because of the strong guide field regime, the qualitative conclusion still holds.

## F. Other related studies about magnetic field generation by shear flows

It is important to mention that previous studies have reported the generation of large scale and long duration magnetic fields as a result of the electron scale kinetic Kelvin-Helmholtz (K-H) instability<sup>37-39</sup>. This instability is closely related to the vortical flow pattern seen in our low PIC guide field runs inside of the secondary magnetic islands. However, these studies were for cold ( $v_{the} \ll V_0$ ) shear flows in unmagnetized plasmas, and therefore do not apply directly to our case. Nevertheless, the physical mechanism that leads to magnetic field generation has many similarities with the one observed in our case. It is based on a current imbalance resulting from the mixing of electrons crossing the deformed shear interface during the non-linear evolution, amplifying any initial magnetic field perturbation in a way similar to the Weibel instability (for unmagnetized anisotropic plasmas). The dynamo process associated with the latter, similar to the seen in our case (See discussion of Fig. 8), is known to work in magnetized environments as well, although less efficiently<sup>40-43</sup>. Note that Weibel instability has also been seen in PIC simulations of magnetic reconnection with a Harris sheet initialization, although without guide field<sup>44,45</sup>.

## VI. FINITE PLASMA BETA EFFECTS

Let us finally discuss the high beta case runs with  $\beta_i = 1.0$ . Although the basic phenomenology is similar, in general the agreement is much better between different guide field PIC runs in the range  $b_g = 1 \rightarrow 10$  and the corresponding GK results. This can be seen in the reconnection rates of Fig. 1(b), as well as in the time evolution of the scaled magnetic fluctuations  $\Gamma\delta B_z$  for the different PIC guide field and GK simulations, shown in Fig. 12(b). The time evolution of the thermal pressure fluctuations  $\Gamma\delta P_{th}$  in Fig. 12(a) displays a different behaviour between the results given by both codes. As we already pointed out, the physical origin of these differences will be analyzed in a follow-up paper.

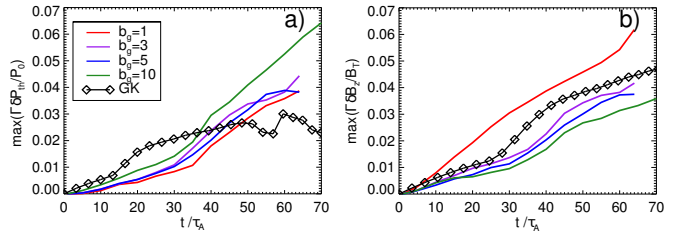
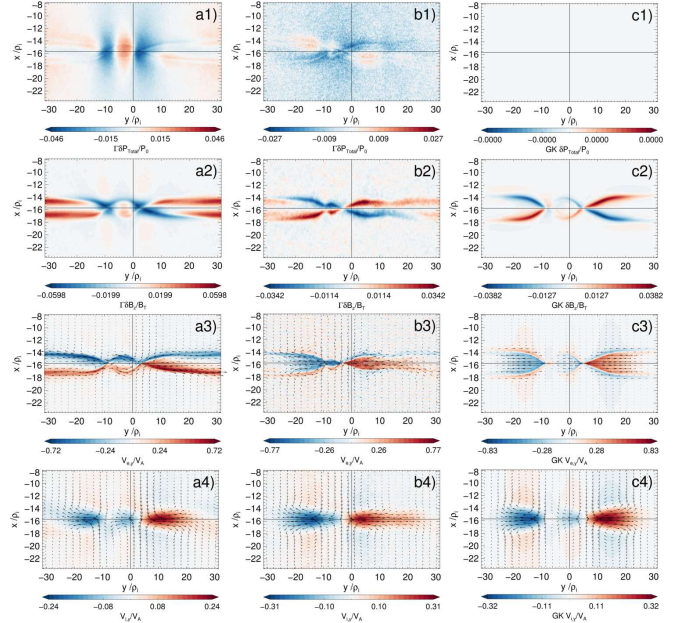


Figure 12. Time history of the maximum value of the scaled thermal  $\Gamma\delta P_{th}/P_{th,0}$  (a) and magnetic fluctuations  $\Gamma\delta B_z/B_T$  (b) for different PIC guide fields and the corresponding GK result, in the high beta case  $\beta = 1.0$ . To be compared with Fig. 5. The scaling factor  $\Gamma$  (Eq.(6)) for the PIC runs was calculated using a reference guide field  $b_{g,ref} = 5$ .

There are at least two related reasons for the better agreement. The first one is because the absolute magnitude of the fluctuating quantities  $\delta P_{th}$  and  $\delta B_z$  are predicted to be smaller by around one order of magnitude compared to the low beta case, since they are proportional to  $\propto 1/\sqrt{\beta}$  (see Eqs. (9) and (10)). In addition, the GK ordering parameter  $\epsilon$  will also be reduced (see discussion of Eq. (7)), improving the validity of the model in this parameter regime. The physical consequences in that the largest deviations from the pressure equilibrium condition will be reduced by the same amount, making more accurate the predictions of the GK approach compared to a Vlasov plasma, and correspondingly the results given by the GK and PIC simulations (see Fig. 13(1st. row)). This also implies that the maximum net force due to the total pressure imbalance in the PIC low guide field regime will be much smaller than in the low beta case.

Second, the range of variation of the Alfvén to ion thermal speed (Eq. (15)), is decreased by a small amount in comparison to the low beta case:  $V_A/v_{th,i} = 0.1 \rightarrow 0.7$  going from  $b_g = 10 \rightarrow 1$ . This means that the Alfvén velocities are always subsonic (even in the extreme case of  $b_g = 0$ , where a comparison between PIC and GK simulations would not make sense). As a result, the maximum values of the initial shear flow will also be subsonic. For the lowest PIC guide field considered,  $b_g = 1$ , the value is  $\max(V_{y0}) \sim 0.3V_A \sim 0.2v_{th,i}$ . Moreover, re-

connection rates are reduced by a factor of two in this regime (see Fig. 1(b)). Then, the maximum electron/ion outflows speeds in units of  $V_A$ , proportional to the reconnection rates, will also be further reduced in comparison to the low beta case, becoming negligible when measured in units of  $v_{th,i}$ . More precisely, we measured maximum electron outflows speeds on the order of  $0.75V_A$  (see Fig. 13(3rd. row)) and ion outflows on the order of  $0.3V_A$  (see Fig. 13(4rd. row)), roughly smaller by a factor of 3 compared with the corresponding values in the low beta case.



The previous observation has two physical consequences. For the GK code, the maximum deviations from the drift approximation where this approach holds, proportional to the maximum speeds in units of  $v_{th,i}$ , will be smaller than in the low beta case (see discussion in Sec. V A). Consequently, a comparison with the PIC runs will be more reliable. For the PIC code, smaller reconnection rates implies less open separatrices and smaller secondary magnetic islands. In the small guide field regime ( $b_g \approx 1$ ) there is still a strong effect of the shear flow around these structures, producing currents (see, e.g., Fig. 13(a3)-(a4)) which become negligible for  $b_g \gtrsim 3$  (see, e.g., Fig. 13(b3)-(b4) for  $b_g = 5$ ). In fact, the Hall term and the corresponding decoupling of electrons and ions is facilitated in high plasma beta environments. That is why we observed in-plane current densities twice as high as the values seen in the low beta case (Fig. 8), as can be calculated from the electron/ion flows in Figs. 13(3rd. row) and Figs. 13(4rd. row). But the generation of core magnetic field, according to the estimate Eq. (16), is proportional to the length scale  $\Delta L$ , which is roughly five times smaller in this case compared to the low beta case (secondary magnetic islands close to the  $X$  point have size around  $\sim 2\rho_i$  across the  $x$  direction, while the magnetic island at  $y$  boundaries has size around  $\sim 4\rho_i$ ). Furthermore, the magnetic field generation due to the colliding outflows at the  $y$  boundaries is decreased, since the maximum outflows speeds are smaller than in the low beta case. This can be seen in the time evolution of  $\Gamma\delta B_z$  in Fig. 12(b), where the deviations are significant only for  $b_g = 1$  and much smaller in absolute terms compared with the low beta case. Convergence with the GK results is already reached with values  $b_g \gtrsim 3$  (see, e.g., the second column of Fig. 13 for  $b_g = 5$ ). This reduction of core magnetic field strength in high  $\beta$  plasmas is in agreement with previous hybrid simulations<sup>19</sup> (although for very low guide fields  $b_g < 1$ ).

Figure 13. Contour plots showing different quantities in the high beta case  $\beta_i = 1.0$  for two PIC guide fields and the corresponding GK result, at a time  $t = 50\tau_A$ . First top row: scaled total pressure  $\Gamma\delta P_{\text{total}}/P_{th,0}$ . a1) PIC  $b_g = 1$ , b1) PIC  $b_g = 5$ , c1) GK. The latter is identically zero to machine precision. Second row: Scaled magnetic fluctuations  $\Gamma\delta B_z/B_T$ . a2) PIC  $b_g = 1$ , b2) PIC  $b_g = 5$ , c2) GK. Third row: Vector plot of the in-plane electron bulk velocity with color coded the component  $V_{e,y}/V_A$ . a3) PIC  $b_g = 1$ , b3) PIC  $b_g = 5$ , c3) GK. Bottom fourth row: Vector plot of the in-plane ion bulk velocity with color coded the component  $V_{i,y}/V_A$ . a4) PIC  $b_g = 1$ , b4) PIC  $b_g = 5$ , c4) GK.

In this point it is important to mention that there is in general a higher level of numerical noise, and associated numerical heating, in this high beta case compared to the low beta one for the PIC runs. It becomes increasingly important for higher guide fields, reducing even faster the signal-to-noise ratio. This is, in part, responsible for the monotonically increasing thermal pressure fluctuations in Fig. 12(a) for later times, especially in the case  $b_g = 10$ . This observation was already pointed out in the original work by Ref. 11, being a well known consequence of the enhanced numerical collisions in weakly magnetized environments simulated by PIC codes, or equivalently, in high beta plasmas<sup>46</sup>.

Therefore, by analyzing a different set of runs in a high  $\beta$  plasma regime, we could distinguish between the different effects of violations of the gyrokinetic ordering in the GK runs and the initial shear flow always present in the PIC force free runs. The first effect is encoded in the parameter  $\epsilon$  (Eq. (7)), which can be as high as 4 in the low beta case for the lowest guide field  $b_g = 5$ . Then, strong deviations from the PIC simulation results are be expected in that regime. On the other hand,  $\epsilon = 0.2$  for the lowest guide field  $b_g = 1$  in the high beta case, and a better agreement is observed. However, we still could find generation of core magnetic field and other phenom-

ena associated with the initial shear flow, although with reduced strength. This also breaks the comparison between PIC to GK, but it does not only rely on the relative value of  $V_A/v_{th,i}$  and other parameter associated to the initial shear flow, but also in the fact that reconnection rates are smaller (less open separatrices and smaller magnetic islands). Thus, we can conclude that a reliable comparison between PIC-GK simulations of magnetic reconnection can be obtained with parameters that provides smaller fluctuations levels (high  $\beta$  plasmas), lower ratios  $V_A/v_{th,i}$  and also relatively small reconnection rates  $d\Psi/dt$  (proportional to  $V_{e,out}/V_A$ , with  $V_{e,out}$  the maximum electron outflow speeds). The balance of this three parameters guarantee a good convergence. However, PIC codes shows an enhanced numerical heating in high  $\beta$  plasmas, making a comparison with GK not so reliable in this regime.

## VII. CONCLUSIONS

By means of fully kinetic PIC and gyrokinetic simulations, we have extended a previous study of magnetic reconnection in the limit of strong guide field<sup>11</sup> using an independent set of PIC and gyrokinetic codes. We established the limits of applicability of gyrokinetic simulations compared to kinetic PIC ones in the low guide field regime, and the physical reasons behind these differences. Note that the following conclusions are based on sets of runs with total ion plasma  $\beta_i = 0.01$  constant for different PIC guide fields.

First, we found the limitations in the linear scaling reported by Ref. 11 in both thermal and magnetic fluctuations for the PIC low guide field regime. These simulations show deviations in the inverse scaling with the guide field compared to the high guide field regime, not converging properly to the gyrokinetic results. These deviations start to be especially significant when secondary magnetic islands start to form, after the reconnection peak time. In this paper we focus on the additional magnetic fluctuations revealed by the PIC low guide field runs, mostly result of macroscopic bulk plasma motions. The analysis of the differences in the thermal fluctuations -that have to do with dissipative processes, heating mechanisms and non thermal effects- will be addressed in a follow-up paper.

More precisely, we found that the PIC low guide field regime shows an excess of magnetic pressure inside of the secondary magnetic islands (core magnetic field), reaching maximum values for times much later than the reconnection peak time. Correspondingly, the agreement between both codes is better before the formation of these structures, during the linear phase of magnetic reconnection. This excess of magnetic pressure is not compensated by a corresponding decrease in the thermal pressure. The numerical reason is that gyrokinetic codes keep the pressure equilibrium condition to machine precision, while PIC codes allow large deviations from it. There-

fore, although the gyrokinetic results can be comparable to the PIC ones for relatively low guide fields ( $b_g = 5, 10$ ) in the separatrices close to the X points, a convergence in the secondary magnetic islands require much higher guide fields ( $b_g \gtrsim 30$ ).

We found that the physical mechanism that generates the core magnetic field is due to an initial shear flow present in the force free PIC initialization. This shear flow, that also produces asymmetric separatrices and reduces reconnection rates, is negligible in the limit of strong guide field and absent in the corresponding gyrokinetic initialization. Through a Hall effect that decouples electron from ion motion, vortical electron flow patterns are generated in the secondary magnetic islands as the magnetic reconnection wraps up magnetic field lines around these structures, carrying the electron shear flow with them. This magnetic field weakens for higher PIC guide field runs, converging to the gyrokinetic result, since the shear flow is not strong enough to drive the currents capable of generating it (when measured in absolute units). There is also an out-of-plane magnetic field generation due to boundary effects in the periodic  $y$  boundaries. PIC runs show a strong magnetic field due to the colliding outflows, non negligible even for stronger guide fields.

The generation of magnetic field inside of the secondary magnetic islands is associated with a dynamo effect ( $\vec{J} \cdot \vec{E} < 0$ ). Moreover, although the islands in the PIC low guide field regime have similar morphology to those formed with much stronger guide fields and the ones seen in the gyrokinetic simulations, they have another fundamental difference. The outflows from the main X point make these islands drift along very quickly, following the bulk flow due to reconnection and not developing their own internal flow patterns.

We also showed that the relative ratio of the electron outflow speed to the ion thermal speed, proportional to  $V_A/v_{th,i}$ , is higher for the PIC low guide field regime, reaching values close to 1 for  $b_g \lesssim 10$ . This breaks the perpendicular drift approximation, a critical assumption in which the gyrokinetic codes (and the gyrokinetic theory in general) are based, and thus an additional source of differences is expected compared to the PIC simulation results.

In spite of all those differences, the gyrokinetic simulations show a development of magnetic reconnection remarkably similar to the PIC high guide field runs. This is of central importance due to the computational savings of the first ones. Indeed, for the low beta case, we measured speed-ups by a factor of  $10^3$  between the gyrokinetic run compared to a corresponding PIC guide field  $b_g = 50$  simulation. However, the computational cost of a PIC simulation decreases linearly with the guide field, in such a way that in the low guide field regime ( $b_g \sim 5$ ), the speed-up and advantages of using gyrokinetic instead of PIC simulations are not so notorious.

Finally, we also analyzed the effects of a high plasma beta  $\beta_i = 1.0$  compared to our standard case  $\beta_i = 0.01$ .

Although the basic phenomenology is similar, we could notice a better agreement between the corresponding PIC and gyrokinetic results, reaching a relatively good convergence for guide fields as low as  $b_g \gtrsim 3$ . From this, we can conclude that an accurate comparison between PIC and gyrokinetic force free simulations of magnetic reconnection requires high plasma  $\beta \sim 1$  (to reduce the fluctuation level proportional to  $1/\sqrt{\beta_i}$ ), although PIC codes are affected by enhanced numerical heating in this regime. Moreover, it is necessary to have parameters with low ratios  $V_A/v_{th,i} \ll 1$  (to avoid the effects of the initial shear flow) and a small ordering parameter  $\epsilon \ll 1$  in the gyrokinetic initialization. In addition, it is also required that reconnection rates should not be too high  $(d\Psi/dt)/\dot{\Psi}_N \lesssim 0.1$ . In the gyrokinetic runs, this is to avoid super-Alfvénic outflows that might break the perpendicular drift approximation. In the PIC runs, this is to avoid to have open separatrices and larger magnetic islands that can facilitate the generation of core magnetic field. The balance of these related numerical and physical parameters allow to determine a convenient parameter regime for an accurate comparison of magnetic reconnection between these plasma models.

## ACKNOWLEDGMENTS

We acknowledge the developers of the code ACRONYM at Würzburg University, the support by the Max-Planck-Princeton Center for Plasma Physics and of the DFG-CRC 963 for P. K. J. B. gratefully acknowledges the support of the German Science Foundation CRC 963. P. M. acknowledges the financial support of the Max-Planck Society via the IMPRS for Solar System Research. The research leading to these results has received funding from the European Research Council under the European Union's Seventh Framework Programme (FP7/2007-2013)/ERC Grant Agreement No. 277870.

## REFERENCES

- <sup>1</sup>J. Büchner, *Plasma Phys. Control. Fusion* **49**, B325 (2007).
- <sup>2</sup>R. A. Treumann and W. Baumjohann, *Front. Phys.* **1**, 31 (2013), arXiv:1401.5995.
- <sup>3</sup>J. Büchner, C. Dum, and M. Scholer, *Space Plasma Simulation* (Springer-Verlag, Berlin Heidelberg, 2003).
- <sup>4</sup>E. A. Frieman and L. Chen, *Phys. Fluids* **25**, 502 (1982).
- <sup>5</sup>A. J. Brizard and T. S. Hahm, *Rev. Mod. Phys.* **79**, 421 (2007).
- <sup>6</sup>W. Wan, Y. Chen, and S. E. Parker, *IEEE Trans. Plasma Sci.* **33**, 609 (2005).
- <sup>7</sup>B. N. Rogers, S. Kobayashi, P. Ricci, W. Dorland, J. Drake, and T. Tatsuno, *Phys. Plasmas* **14**, 092110 (2007).
- <sup>8</sup>M. J. Pueschel, F. Jenko, D. Told, and J. Büchner, *Phys. Plasmas* **18**, 112102 (2011).
- <sup>9</sup>M. J. Pueschel, D. Told, P. W. Terry, F. Jenko, E. G. Zweibel, V. Zhdankin, and H. Lesch, *Astrophys. J. Suppl. Ser.* **213**, 30 (2014).
- <sup>10</sup>E. G. Harris, *Nuovo Cim.* **23**, 115 (1962).
- <sup>11</sup>J. M. TenBarge, W. Daughton, H. Karimabadi, G. G. Howes, and W. Dorland, *Phys. Plasmas* **21**, 020708 (2014), arXiv:1312.5166.
- <sup>12</sup>B. N. Rogers, R. E. Denton, J. F. Drake, and M. A. Shay, *Phys. Rev. Lett.* **87**, 195004 (2001).
- <sup>13</sup>L. Chen, W. Daughton, and A. Bhattacharjee, *Phys. Plasmas* **19**, 112902 (2012).
- <sup>14</sup>M. Zhou, X. H. Deng, and S. Y. Huang, *Phys. Plasmas* **19**, 042902 (2012).
- <sup>15</sup>S. Y. Huang, M. Zhou, Z. G. Yuan, X. H. Deng, F. Sahraoui, Y. Pang, and S. Fu, *J. Geophys. Res. Sp. Phys.* **119**, 7402 (2014).
- <sup>16</sup>C. Huang, Q. Lu, M. Wu, S. Lu, and S. Wang, *J. Geophys. Res. Sp. Phys.* **118**, 991 (2013).
- <sup>17</sup>J. F. Drake, M. Swisdak, K. M. Schoeffler, B. N. Rogers, and S. Kobayashi, *Geophys. Res. Lett.* **33**, L13105 (2006).
- <sup>18</sup>W. Daughton, V. Roytershteyn, H. Karimabadi, L. Yin, B. J. Albright, S. P. Gary, K. J. Bowers, and S. Consistent, in *AIP Conf. Proc.*, Vol. 1320 (2011) p. 144.
- <sup>19</sup>H. Karimabadi, D. Krauss-Varban, N. Omidi, and H. X. Vu, *J. Geophys. Res.* **104**, 12313 (1999).
- <sup>20</sup>M. Zhou, Y. Pang, X. Deng, S. Huang, and X. Lai, *J. Geophys. Res. Sp. Phys.* **119**, 6177 (2014).
- <sup>21</sup>P. A. Cassak and M. A. Shay, *Space Sci. Rev.* **172**, 283 (2011).
- <sup>22</sup>V. Roytershteyn and W. Daughton, *Phys. Plasmas* **15**, 082901 (2008).
- <sup>23</sup>M. Hosseinpour and M. a. Mohammadi, *Phys. Plasmas* **20**, 114501 (2013).
- <sup>24</sup>Z. Wang, P. L. Pritchett, and M. Ashour-Abdalla, *Phys. Fluids B Plasma Phys.* **4**, 1092 (1992).
- <sup>25</sup>R. L. Fermo, J. F. Drake, and M. Swisdak, *Phys. Rev. Lett.* **108**, 255005 (2012).
- <sup>26</sup>P. Kilian, T. Burkart, and F. Spanier, in *High Perform. Comput. Sci. Eng. '11*, edited by W. E. Nagel, D. B. Kröner, and M. M. Resch (Springer Berlin Heidelberg, Berlin, Heidelberg, 2012) pp. 5–13.
- <sup>27</sup>F. Jenko, W. Dorland, M. Kotschenreuther, and B. N. Rogers, *Phys. Plasmas* **7**, 1904 (2000).
- <sup>28</sup>P. Ricci, J. U. Brackbill, W. Daughton, and G. Lapenta, *Phys. Plasmas* **11**, 4102 (2004).
- <sup>29</sup>Y.-H. Liu, W. Daughton, H. Karimabadi, H. Li, and S. Peter Gary, *Phys. Plasmas* **21**, 022113 (2014).
- <sup>30</sup>A. Stanier, A. N. Simakov, L. Chacón, and W. Daughton, *Phys. Plasmas* **22**, 010701 (2015).
- <sup>31</sup>P. A. Cassak, R. N. Baylor, R. L. Fermo, M. T. Beidler, M. A. Shay, M. Swisdak, J. F. Drake, and H. Karimabadi, *Phys. Plasmas* **22**, 020705 (2015), arXiv:1502.01781v1.
- <sup>32</sup>B. N. Rogers, *J. Geophys. Res.* **108**, 1111 (2003).
- <sup>33</sup>P. A. Cassak, *Phys. Plasmas* **18**, 072106 (2011).
- <sup>34</sup>Q. Q. Shi, Z. Y. Pu, H. Zhang, S. Y. Fu, C. J. Xiao, Q. G. Zong, T. A. Fritz, and Z. X. Liu, *Surv. Geophys.* **26**, 369 (2005).
- <sup>35</sup>T. K. M. Nakamura, M. Fujimoto, and A. Otto, *J. Geophys. Res. Sp. Phys.* **113**, A09204 (2008).
- <sup>36</sup>M. A. Shay, J. F. Drake, B. N. Rogers, and R. E. Denton, *J. Geophys. Res.* **106**, 3759 (2001).
- <sup>37</sup>E. P. Alves, T. Grismayer, S. F. Martins, F. Fiúza, R. a. Fonseca, and L. O. Silva, *Astrophys. J.* **746**, L14 (2012).
- <sup>38</sup>T. Grismayer, E. P. Alves, R. A. Fonseca, and L. O. Silva, *Phys. Rev. Lett.* **111**, 015005 (2013).
- <sup>39</sup>E. P. Alves, T. Grismayer, R. Fonseca, and L. O. Silva, *New J. Phys.* **16**, 035007 (2014), arXiv:1404.0555.
- <sup>40</sup>M. V. Medvedev and A. Loeb, *Astrophys. J.* **526**, 697 (1999).
- <sup>41</sup>C. B. Hededal and K.-I. Nishikawa, *Astrophys. J.* **623**, L89 (2005).
- <sup>42</sup>A. Stockem, I. Lerche, and R. Schlickeiser, *Astrophys. J.* **651**, 584 (2006).
- <sup>43</sup>R. C. Tautz and A. Shalchi, *Phys. Plasmas* **15**, 052304 (2008).
- <sup>44</sup>S. Lu, Q. Lu, X. Shao, P. H. Yoon, and S. Wang, *Phys. Plasmas* **18**, 072105 (2011).
- <sup>45</sup>K. M. Schoeffler, J. F. Drake, M. Swisdak, and K. Knizhnik,

*Astrophys. J.* **764**, 126 (2013).

<sup>46</sup>Y. Matsuda and H. Okuda, *Phys. Fluids* **18**, 1740 (1975).